Journal of Hazardous Materials 493 (2025) 138373

Contents lists available at ScienceDirect

Journal of Hazardous Materials

journal homepage: www.elsevier.com/locate/jhazmat

eResearch Paper

Ligand-limited oxidation of ciprofloxacin by Mn(III)

Tra My Bui Thi [a,1], Tao Chen [a,1], Tao Luo [b], Yann Leroux [c], Khalil Hanna [a], Jean-François Boily [b,*]

[a] Univ. Rennes, Ecole Nationale Supérieure de Chimie de Rennes, CNRS, ISCR-UMR 6226, Rennes F-35000, France
[b] Department of Chemistry, Umeå University, Umeå SE-901 87, Sweden
[c] Univ. Rennes, CNRS, ISCR-UMR 6226, Rennes F-35000, France

HIGHLIGHTS

- Mn(III) species influence the environmental fate of antibiotics.
- Mn(III) complexation with pyrophosphate inhibits ciprofloxacin degradation.
- Mn(III)-PP complexes dissociate into aqueous Mn(III) species and form MnO_2 colloids.
- pH altered the redox potential of the Mn(III)/Mn(II) couple, affecting CIP degradation.

GRAPHICAL ABSTRACT

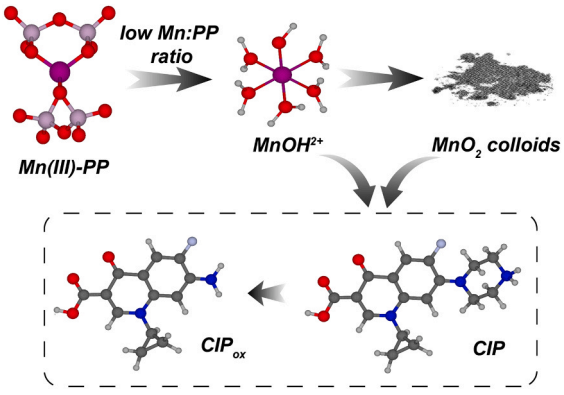

ARTICLE INFO

Keywords:
Manganese
Ciprofloxacin
Oxidation
Aqueous speciation
Spectroscopy

ABSTRACT

Mn(III) species play critical roles in determining the environmental fate of antibiotics released into natural systems. However, their reactivity is strongly influenced by complexation reactions with (in)organic ligands. This study investigates the impact of Mn(III) complexation with pyrophosphate (PP), a model environmental ligand, on the redox-driven degradation of ciprofloxacin (CIP), a widely used antibiotic and environmental contaminant. Spectroscopic analysis and thermodynamic modeling revealed that Mn(III)-PP complexes initially dissociate into $MnOH^{2+}$ species, which can then disproportionate and form MnO_2 colloids. Both dissociation and disproportionation reactions had comparable trends at pH 4 and 7, with reactivities that were strongly dependent on Mn(III):PP ratios. The progress of CIP oxidation following direct coordination with Mn compounds over time was sigmoidal, with an initial lag phase attributed to Mn(III)-PP complex dissociation and disproportionation. CIP degradation was predominantly governed by pH, with maximal rate constants decreasing from $k = 0.390\ h^{-1}$ at pH 3 to $k = 0.065\ h^{-1}$ at pH 5, and no CIP removal under circumneutral to alkaline conditions. Cyclic voltammetry also confirmed that the strongly pH-dependent redox potential of the Mn(III)/Mn(II) couple aligned with facile CIP oxidation under acidic conditions. These collective findings indicated that ligand complexation, such as with PP, enhanced Mn(III) stability and mitigated dissociation and disproportionation reactions. The new

* Corresponding author.
E-mail address: jean-francois.boily@umu.se (J.-F. Boily).
[1] These authors contribute equally to this work and are designated as co-first authors.

https://doi.org/10.1016/j.jhazmat.2025.138373
Received 11 February 2025; Received in revised form 4 April 2025; Accepted 21 April 2025
Available online 22 April 2025
0304-3894/© 2025 The Author(s). Published by Elsevier B.V. This is an open access article under the CC BY license (http://creativecommons.org/licenses/by/4.0/).

insight provided by this work on the speciation and redox activity of Mn(III) should thereby be considered for understanding ciprofloxacin degradation in contaminated water systems.

1. Introduction

Mn(III) is an abundant and highly reactive component in the natural pool of manganese. It serves both as an electron donor and acceptor [1,2], playing an important role in various biogeochemical and water treatment processes [3–6]. Mn(III) appears to make up the majority of the (μM-level) dissolved pool of Mn in suboxic water columns of the Black [1] and Baltic [7] Seas. In England, soluble Mn(III) was also produced in a water treatment plant by reacting natural organic matter (NOM) with Mn oxides [4]. Although seemingly overlooked in the past decades, the complexation of soluble Mn(III) to (in)organic ligands could affect manganese redox cycling in natural waters [1,7–10]. For instance, Kostka et al. [11] highlighted the possibility that complexation with pyrophosphate (PP) affects the ability of Mn(III) to act as a terminal reactant in aquatic environments. Variations in Mn(III)-ligand (L) speciation could also play important roles in the fate of redox-active organic pollutants of great concern to society, such as antibiotics.

Mn(III)-L complexes are well-known intermediates in the degradation of organic contaminants. Reactions can occur through permanganate reduction with bisulfite [12,13], abiotic and biotic Mn(II) oxidation [14–18], and through Mn (IV) minerals [16,18] exposed to complexing ligands. For instance, Gao et al. [13] found that Mn(III)-L generation by Mn(VII)/Mn(II) reactions in the presence of PP or humic acid accelerated triclosan oxidation rates. Chen et al. [16] also reported that complexation with Mn(III)-oxalate complexes affected carbadox stability. Additionally, work on UO_2 dissolution by Mn(III) suggested that coordination structure impacted the ability to control binding capacity and heterogeneous electron transfer [19].

Present in naturally occurring ligands (e.g., NOM [4,5], biogenic siderophores [14,20], carboxylate [21]), phosphonate groups can act as an important stabilizer for soluble Mn(III) [21–23] in environmental and industrial settings (e.g., agricultural areas, domestic sources, and industrial facilities) [24–26]. Previous studies revealed that aqueous Mn (III)-PP complexes, which are stabilized by direct Mn-phosphate interactions, could greatly enhance the oxidative reactivity of MnO_2 [13,18,27], yet the same species inhibited phenol oxidation [28]. Although ligand exchange should be the chief mechanism for organic pollutant oxidation by Mn(III)-L complexes [12–14,29–31], uncertainties remain over Mn(III) coordination structures, speciation, and redox activities.

In this study, we evaluated the ability of PP to regulate the structure and redox behaviors of Mn(III) complexes towards the degradation of ciprofloxacin (CIP). The interest for the fate of this important fluoroquinolone antibiotic has spiked in recent years, given its release to the environment [32,33] from activities in the pharmaceutical and livestock sectors [34–37]. The concern becomes even greater considering that metal-driven oxidation of CIP produces other compounds [38–40] of yet unknown antibacterial properties. To address these concerns, we developed a kinetic model describing the autocatalytic nature of the Mn (III)-driven oxidation of CIP, and explained how Mn(III)-PP complexes inhibit degradation. This study contributes to the growing body of literature on the reactivity of dissolved Mn(III) towards organic pollutants [6,41,42], while at the same time adding new insight needed to reframe our understanding of Mn redox cycling in nature.

2. Methods

2.1. Materials

Manganese(III) acetate dihydrate ($(CH_3COO)_3Mn{\cdot}2H_2O$) and sodium pyrophosphate decahydrate ($Na_4P_2O_7{\cdot}10H_2O$) were purchased from Sigma-Aldrich, and used as received. A thermodynamically stable Mn (III)-PP stock solution was prepared following a procedure from the literature [22,23]. All Mn(III)-L stock solutions were made in N_2(g)-sparged anoxic ultrapure water (18.2 MΩ cm). These were prepared by mixing 10 mM Mn(III) acetate powder with alkaline solutions of 20–100 mM sodium pyrophosphate decahydrate, while stirring with a magnetic stirrer. This procedure produced pH ~ 7 solutions of Mn (III)-PP complexes at Mn(III):PP ratios in the 1:2–1:10 range. The pH of the original PP solutions was thereafter adjusted using 0.1 M HCl or 0.1 M NaOH.

Freshly-prepared solutions of Mn(III):PP ratios lower than 1:4 were immediately filtered (0.22 μm hydrophilic polytetrafluoroethylene, H-PTFE-20/13, Duren-Germany) to minimize rapid Mn(III) disproportionation, and to avoid the influence of interfering solid substances on the reaction process. Those at Mn(III):PP ratios of 1:4 and higher were filtered and stored in the dark in a refrigerator at 4 °C. The half-lives of those solutions ranged from about 25 to 530 days, depending on Mn:PP ratios [22,23]. Standard solutions of Mn(III)-PP complexes at concentrations of 10, 50, 100, 200, 500, and 1000 μM were then prepared in triplicates by dilution of a 10 mM Mn(III)-PP stock solution at a Mn:PP ratio of 1:5. The stock solution concentration was measured before each experiment to ensure that no decomposition occurred. These values were measured using an ultraviolet-visible (UV-Vis) spectrophotometer (Cary-50, Varian).

2.2. CIP oxidation

The time-resolved oxidation of CIP by Mn(III) was studied in 200 mL solutions, which were stirred at 25 °C in 250 mL Nalgene bottles open to the atmosphere in the absence of light. The solutions were prepared by adding aliquots of the CIP and Mn(III)-PP stock solutions to the reaction vessel. To minimize Mn(III) disproportionation, solution pH was adjusted to pre-selected values by adding aliquots of 0.1 M HCl or 0.1 M NaOH. The resulting solutions contained 20 μM CIP, 200–800 μM Mn (III), and PP at Mn:PP ratios of 1:2–1:10. The pH was not controlled during the course of the reactions, as excess PP buffered the solutions (pK_a = 0.85, 1.96, 6.60, and 9.41) [43]. Aliquots of 2 mL were periodically collected from the reaction vessel, and the reactions were promptly quenched by adding 10 μL of a 1 M hydroxylamine hydrochloride solution.

To examine the reactivity of colloidal MnO_2 from Mn(III) dissociation, the disproportionation of 100 μM Mn(III)-PP complexes was studied in a 7-h reaction at pH 4 and 7. Samples were taken at specific time intervals, and concentrations of Mn(III)-PP and MnO_2 colloids were analyzed immediately without filtration or quenching. A 20 μM CIP was thereafter added to evaluate the oxidation capacities of Mn(III) and MnO_2 colloids. Note that pH was not altered by Mn(III) disproportionation or CIP addition due to PP buffering. The CIP-containing suspensions were then periodically sampled, filtered, and quenched prior to CIP concentration measurements. As a control experiment, the oxidation of a 20 μM CIP solution mixed in a suspension containing 100 μM acid birnessite (δ-MnO_2) suspensions was studied at pH 4 and 7 at 0 and 1 mM PP. This δ-MnO_2 (specific surface area 85.0 ± 3.0 m^2/g) was prepared and characterized by Li et al. [44]. All batch experiments were conducted under an open atmosphere and in the dark by covering the Nalgene bottles with aluminum foil. All the kinetic experiments were performed in triplicates at room temperature (25 ± 2 °C).

2.3. Aqueous species determination

Aqueous CIP concentrations were determined using a high-performance liquid chromatograph (Waters 600 controller) equipped

with a reversed-phase C18 column (250 mm × 4.6 mm i.d., 5 μm) and a UV detector (Waters 2489). The mobile phase was a mixture of acetonitrile/water (25/75 v/v) containing 0.1 % formic acid. The UV detector was set to 275 nm for CIP. CIP oxidation byproducts were thereafter analyzed using a Waters Ultra High-Pressure Liquid Chromatography-Mass Spectrometer (HPLC-MS; Acquity UPLC) system equipped with a Waters BEH C18 column (100 mm × 2.1 mm, 1.7 μm) and a mass spectrometer. The mobile phase consisted of acetonitrile containing 0.1 % formic acid (eluant A) and a 10%/90% acetonitrile/water mixture containing 0.1 % formic acid (eluant B), with a working gradient of 0 min/0 % A−1 min/0 % A−9 min/100 % A−12 min/ 0 % A, and a flow rate of 400 μL min^{-1}. An electrospray interface (ESI) was used for the MS measurements in positive ionization mode and full scan acquisition.

The disappearance of Mn(III)-PP complexes and the formation of colloidal MnO_2 in Mn(III) disproportionation experiments were monitored by UV-Vis spectrophotometry using a 10 mm light path quartz cuvette. Full-range scans in the 200 – 800 nm range were conducted to exclude background shifts from light scattering that could have possibly occurred by the formation of colloidal MnO_2 [45,46]. All sample absorbances were corrected by subtracting the blank absorbance of distilled water.

2.4. Electrochemical potentials

Cyclic voltammetry (CV) was used to determine the half-wave potentials ($E_{1/2}$) of Mn(III)-PP complexes. Experiments were carried out in 100 mM NaCl solutions containing 1 mM Mn(III)-PP at pH 3–7, and with Mn(III):PP ratios from 1:2 to 1:10. All data were collected with a scan range between − 1.0 V and + 1.0 V at a scan rate of 100 mV/s using a three-electrode system consisting of a glassy carbon as the working electrode, a platinum electrode as the counter electrode, and a saturated calomel electrode (SCE) or Ag/AgCl/KCl as the reference electrode. The half-wave potential ($E_{1/2}$) was used as an approximation of the formal potential ($E^{0'}$) of the redox system:

$$E_{1/2} = \frac{1}{2}(E_{pa} + E_{pc}) \quad (1)$$

and where E_{pa} and E_{pc} are respectively the anodic and cathodic peak potentials.

2.5. Vibrational spectroscopy

Fourier Transform Infrared (FTIR) spectroscopy was used to collect the vibrational spectra of Mn(III)-PP complexes in freshly prepared and filtered solutions of 20 mM Mn(III)-PP at Mn(III):PP ratios of 1:2–1:10. All spectra were acquired immediately after adjusting pH between 3 and 7. All measurements were made on 10 μL aliquots of freshly-prepared solutions using an Attenuated Total Reflectance (ATR) accessory (single-reflection diamond window, Golden Gate by Specac). The spectra were collected at a resolution 4 cm^{-1} in the 600–4500 cm^{-1} range, and at a forward/reverse scanning rate of 10 kHz using a Bruker Vertex 70/v FTIR spectrometer equipped with a DLaTGs detector.

Spectral analyses were subsequently focused on the 800–1400 cm^{-1} range, which covers the main P-O(H) vibrational bands of PP [47]. All resulting spectra were offset by a linear baseline anchored at 800 and 1400 cm^{-1}, but were not normalized for absorbance. The spectral contributions of the water bending region (~1630 cm^{-1}) were thereafter subtracted using the spectra of matrix-matched samples without PP. The resulting matrix ($\boldsymbol{A}$) of spectra collected over several pH and/or Mn:PP ratios where then expressed in terms of a linear combination of the product of spectral ($\boldsymbol{\varepsilon}$) and concentration ($\boldsymbol{C}$) profiles, namely through the Beer-Lambert law ($\boldsymbol{A} = \boldsymbol{\varepsilon_n C_n}$). This was achieved using the program MCR-ALS [48] in the computational environment of MATLAB (The Mathworks, Inc.). The approximate number (n) of spectral components to be considered by MCR-ALS was obtained by evaluating the dimensionality of $\boldsymbol{A}$ using the Factor Indicator Function [49] and by inspecting the lengths of linearly-independent components obtained by singular value decomposition (SVD). This number of component was then used for MCR-ALS. In support for the validity of the results, MCR-ALS analyses conducted at greater values of n produced redundant spectral components $\boldsymbol{\varepsilon}$, while analyses at smaller values of n did not reproduce the variance in the data. These efforts extracted the salient spectral profiles needed to interpret of plausible complexation structures of Mn(III)-PP complexes.

2.6. MCR analysis of UV-Vis spectra

Concentration profiles of Mn(III)-PP and MnO_2 colloids in Mn(III) disproportionation experiments were also extracted by MCR. The MCR analysis on the time-resolved UV-Vis spectra produced spectral fingerprints (Fig. S9c) and absorbance intensity profiles (Fig. S10) for both Mn:PP ratios of 1:5 and/or 1:2, at pH 4 and pH 7. Concentration profiles were then obtained using molar absorptivities at 258 nm for Mn(III)-PP ($\varepsilon_{258\ nm} = 6100\ M^{-1}\ cm^{-1}$) [45,46] and at 368 nm for MnO_2 colloids ($\varepsilon_{370\ nm} = 9180\ M^{-1}\ cm^{-1}$) [45,50]. In particular, MnO_2 concentrations were calculated with $[MnO_2] = A_{370\ nm}/\varepsilon_{370\ nm}$, and residual Mn(III)-PP concentrations with $[Mn(III)\text{-}PP] = A_{258\ nm}/\varepsilon_{258\ nm}$ (*cf.* Fig. S10 for $A_{370\ nm}$ and $A_{258\ nm}$).

2.7. Thermodynamic calculations

Speciation calculations of Mn(III)-PP solutions at Mn:PP ratios of 1:2 and 1:5 studied by FTIR (20 mM Mn(III)) and in CIP degradation experiments (200 μM Mn(III)) were performed using critically selected and experimentally calibrated equilibrium constants (Table S3) [23]. Geochemical speciation calculations were made using PHREEQC (version 2) [51]. Mn redox and PP hydrolysis reactions were not considered in these calculations to focus on the initial conditions and possible reactive intermediates. Note that the calculations were conducted for a simplified simulated system in the absence of CIP, and information on reaction kinetics was not included. The speciation calculations therefore only represented the final equilibrated states of each component. The kinetic behaviors of Mn(III) disproportionation were, additionally, studied in supplement to our thermodynamic calculations.

3. Results and discussion

3.1. Reactivity of soluble Mn(III)-PP towards CIP oxidation

Variations in Mn(III) concentration, pH, and Mn(III):PP ratio played the following key roles in the kinetics of CIP removal from aqueous solutions (Fig. 1). CIP concentrations were unaffected by Mn(III):PP ratios at and above 1:5, regardless of concentration or pH (Fig. 1(a,b)). This was confirmed further by experiments at pH 4 (Fig. 1c), showing that CIP removal was effective at lower ratios. Time-resolved batch experiments also revealed that Mn(III)-PP reactivity was facilitated only in the pH 3–5 range, while no reactivity took place at pH 7 and 9 (Fig. 1b).

The sigmoidal shape of the time-resolved removal of CIP, marked by an initial lag phase followed by an exponential degradation phase, was suggestive of an autocatalytic process also seen in previous Mn(III)-driven organic removal studies [41,42,52]. The data were modeled using a reparametrized Gompertz kinetic model by non-linear regression fitting of the data [53]:

$$\frac{C}{C_0} = 1 - e^{-e^{ke(\lambda - t)+1}} \quad (2)$$

where k (h^{-1}) is the maximum reaction rate, λ (h) is the lag phase duration, and C_0 is the initial and C the final CIP concentration. The

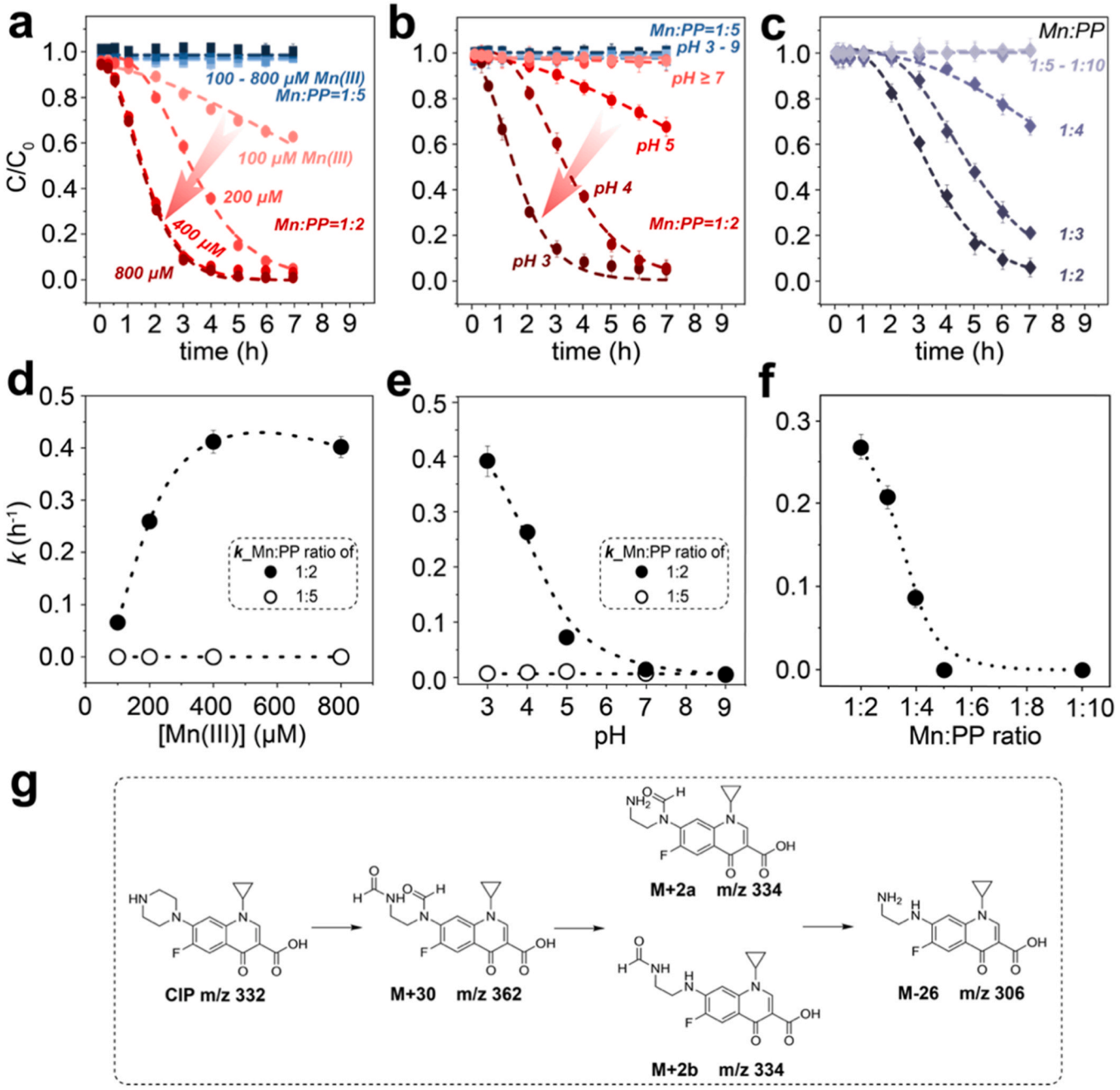

Fig. 1. CIP removal kinetics from solutions of $C_0 = 20$ μM CIP and dependence of CIP removal rates (k of Eq. (2)) in the presence of (a,d) 100–800 μM Mn(III) at pH 4 at Mn:PP ratios of 1:2 (red) and 1:5 (blue), (b,e) 200 μM Mn(III) at pH 3–9 at Mn:PP ratios of 1:2 (red) and 1:5 (blue), (c,f) 200 μM Mn(III) at Mn:PP ratios from 1:2–1:10 at pH 4. Dashed lines are predictions from the Gompertz model (Eq. (2)). (g) CIP oxidation by-products after a 7-h of reaction with 20 μM CIP, 200 μM Mn (III) at a Mn:PP ratio of 1:2 at pH 4.

statistical indicator of the quality of the fit, the regression coefficient of determinations (R^2), was reported in Table S1. The resulting model parameters captured the concept of CIP decomposition in relation to concentration, pH, and Mn:PP ratios (Fig. 1d–f and Table S1). Notably, decomposition rates were sufficiently high at Mn:PP ratios only below 1:5, with values scaling with Mn(III) concentration. These values plateaued at ~ 400 μM ($k = 0.4\ h^{-1}$) and had shorter lag durations (Fig. S1). Removal rates were, additionally, only significant at pH values below ~ 6 (Fig. 1e).

This pH dependence also aligns with cyclic voltammetry measurements (*cf.* Fig. S2 and Table S2), which revealed half-wave potentials ($E_{1/2}$) from 0.75 V at pH 5 down to 0.4 V at pH 9. As higher $E_{1/2}$ values signaled solutions of greater electron transfer capability [54], these findings add support to our kinetic results and models showing that acidic solutions (pH 3–6) had a greater propensity for CIP oxidation than more alkaline solutions. Also, from speciation calculations (Fig. S3) [22] showing that acidic conditions favored free PP species, these findings support the concept that CIP oxidation was driven by un-complexed Mn species.

CIP degradation products, which we identified by HPLC-MS, included four compounds resulting from the dealkylation of the piperazine group (Fig. 1g). As previously shown in CIP degradation studies [38,55], direct coordination between CIP functional (carboxyl and ketone) groups and a redox-active metal ion center or surficial high-valent metal [39,55,56], were needed to initiate electron transfer reactions.

Our kinetic analysis thus offered insightful observations into the

effects of Mn:PP ratio and pH on CIP oxidation. In the following section, we will turn to vibrational spectroscopy to resolve the molecular-level mechanisms controlling Mn(III)-PP stability. This will provide clues on the role of PP complexation in controlling the availability of redox-active Mn species in relation to CIP removal.

3.2. Stoichiometry and coordination structure

To assess how Mn:L ratios and pH controlled Mn(III) speciations, we probed functional groups of Mn(III)-PP complexes using ATR-FTIR spectroscopy (Fig. 2). These efforts were focused on fresh solutions at Mn:PP ratios from 1:2 to 1:10 at pH 7, where Mn(III)-PP complexes are stable [22]. From thermodynamic predictions of multiple equilibrium constants (Table S3, Fig. S3) and experiments [23,57], these solutions contained various concentrations of uncomplexed PP (PP_{free}) species, alongside the dominant $Mn(PP)_2^{5-}$ complex.

Using the P-O stretching region as a primary marker for coordination, we found that the major band intensities (907, 954, and 1108 cm^{-1}) scaled with Mn:PP ratios (Fig. 2a). MCR showed that the variance in these band intensities could be explained using three spectral components (Fig. 2b) [48]. Component MCR_a I remained relatively constant over Mn:PP ratios while MCR_a II and MCR_a III scaled with ligand concentrations. Comparison with thermodynamic predictions (Fig. S3) supported the concept that MCR_a I was from $MnPP_2^{5-}$ and that MCR_a II and MCR_a III were from PP_{free} species. This assignment aligns with (i) a ~1060 cm^{-1} band that was absent in free PP species and representing P-O-Mn(III) formation (Fig. 2, S4, Table S4), and (ii) the lack of response to deuteration (Fig. S5) which indicated that the species was deprotonated. By comparing the spectra of free PP species at pH 7 and 8, we assigned MCR_a II to H_2PP^{2-} and MCR_a III to HPP^{3-} (Table S4 and Figs. S4-S5).

This assignment was supported further by linear correlations between MCR absorbances and species concentrations (Fig. S6), as well as from the response of their bands to protonation (Fig. S4). In line with their concentration profile, the redox potentials of Mn(III)-PP complexes remained unchanged with variations in Mn(III):PP ratios (Fig. S2, and Table S2). This consequently strengthened our assignment of a 1:2 stoichiometry for Mn(III)-PP complex, even in the presence of excess PP. This also implied that all Mn(III) were in the form of the $MnPP_2^{5-}$ complex (Fig. S3).

In light of these findings, we propose that $MnPP_2^{5-}$ was the chief Mn(III)-PP complex [23] limiting the availability of the redox-active Mn species in aqueous solutions. Judging from the expectation that the Jahn-Teller distortion of the $Mn(III)O_6$ coordination environment involves an elongation of two axial Mn-O bonds and the shrinkage of four equatorial ones [58], the Mn^{3+} center of the $MnPP_2^{5-}$ complex is likely chelated by four terminal phosphate oxygens (Fig. 2e). The coordination structure of $MnPP_2^{5-}$, agrees well with numerical simulations of mineral surface-bound PP in a preferred mononuclear bidentate configuration [59] and Mn(III)-oxalate/uranium-PP structures [60,61]. Although the molecular orbitals of Mn(III) should not be fully occupied, elongated Mn-O bonds could only be accessible for monodentate water molecules. If this is the case, then the $MnPP_2^{5-}$ complex should be inactive towards CIP oxidation when the Mn^{3+} center is unavailable for coordination with CIP.

With these concepts in mind, we can now gain information on CIP

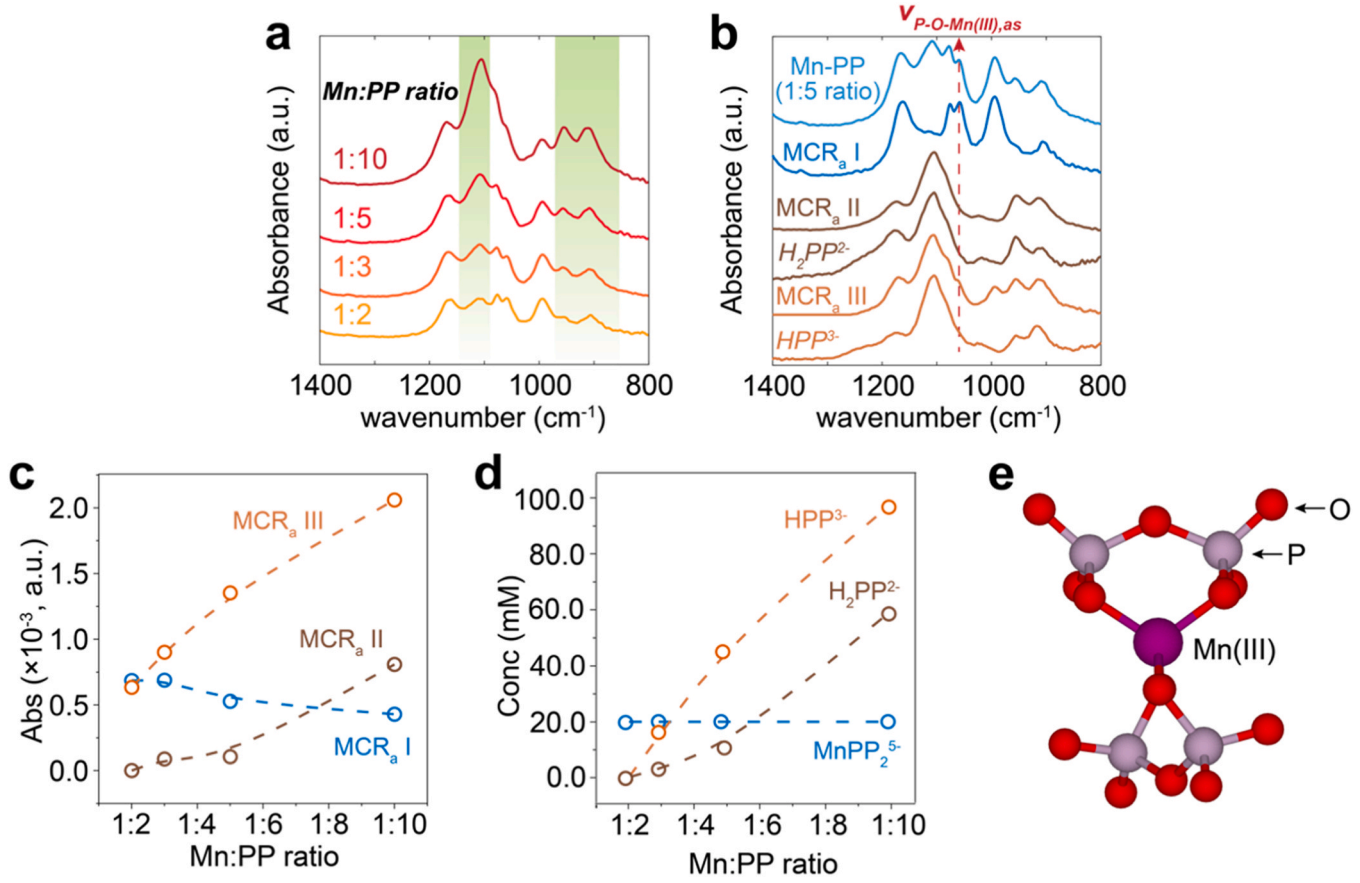

Fig. 2. (a) ATR-FTIR spectra of the P-O stretching region of 20 mM Mn(III) solutions at Mn:PP ratios from 1:2 to 1:10 at pH 7. (b-c) MCR analyses of these spectra generated MCR_a (b) spectral and (c) concentration profiles. Reference spectra of the free H_2PP^{2-} and HPP^{3-} and of the complexed $MnPP_2^{5-}$ (Mn:PP ratio of 1:5) species are shown in (b) for comparison. (d) Concentrations profiles of Mn(III)-PP species generated by thermodynamic calculations (Table S3) for the same solution compositions in (a) are directly comparable to MCR concentration profiles in (c). (e) A proposed possible coordination structure of the $MnPP_2^{5-}$ complex.

oxidation pathways made possible in solutions of lower Mn:PP ratios and lower pH (Fig. 1). MCR analyses of FTIR spectra of solutions (Fig. 3) captured this by showing a strong dependence of pH and Mn:PP ratios on $MnPP_2^{5-}$ stability. This was seen through the loss of the ~1060 cm^{-1} band from the asymmetric stretch of the P-O-Mn(III) bond in acidic media (Fig. 3a, d), which signaled the presence of the uncomplexed $MnOH^{2+}$ species (Fig. S3). Of note, MCR extracted two components at Mn:PP = 1:2 (MCR_c I = $MnPP_2^{5-}$; MCR_c II = PP_{free}), yet three components were needed for Mn:PP = 1:5 (MCR_b I = $MnPP_2^{5-}$ + PP_{free}; MCR_b II = $MnPP_2^{5-}$; MCR_b III = PP_{free}) because of an excess of uncomplexed PP in those solutions.

The resulting MCR concentration profiles (Fig. 3c, f) revealed speciation changes at different pH values. Alongside our thermodynamic predictions (Fig. S3), these analyses confirmed that CIP oxidation reactions were only possible outside the stability field of the $MnPP_2^{5-}$ complex. This is a stability field where Mn speciation is dominated by hydrolyzed $MnOH^{2+}$ and other Mn products from $MnOH^{2+}$ disproportionation.

These results consequently indicated that shifting pH destabilized Mn(III)-PP complexes, and that solutions of lower Mn:PP ratio were more favorable to Mn(III) dissociation. Clear indications for speciation changes facilitating CIP oxidation will be discussed in the following section by linking speciation calculations to dissociation kinetics.

3.3. Kinetic of reactive Mn species formation

To identify the reactive Mn species driving CIP decomposition, we compared the chemical speciation of solutions used for our decomposition (200 μM Mn(III); Fig. S7b) with those used in our FTIR work (20 mM Mn(III); Fig. S7a). These calculations revealed that the Mn(III)-PP complex was replaced by a hydrolyzed species $MnOH^{2+}$ under acidic but to $Mn(OH)_3$ under alkaline conditions (Fig. S3). As CIP decomposition occurred only below pH ~ 5.5 (Fig. 1e, S7b), we propose that CIP removal could be partly driven by interactions with $MnOH^{2+}$. This species facilitated decomposition as the Mn(III) ion can be directly coordinated by CIP functional (carboxyl and ketone) groups, in contrast to the Mn(III)-PP species where Mn(III) is completely surrounded by PP functional groups (Fig. 2e). Coordination with CIP functional groups is thus expected to facilitate the electron transfer reaction (Mn(III) → Mn(II)) needed for CIP oxidation (CIP → CIP_{ox}, Fig. 1g). The redox reactivity of $MnOH^{2+}$ originated from the greater delocalization of electrons in Mn^{3+} caused by complexation with the polarizable OH^- ligand. This strong redox capacity can also be understood from the higher redox potential of Mn(III) (E_H° (Mn^{3+}/Mn^{2+}) = 1.51 V) compared to that of solid Mn(IV) (E_H° (MnO_2/Mn^{2+}) = 1.23 V) [11,62]. Our interpretation that Mn(III)-PP conversion to $MnOH^{2+}$ leads to CIP degradation aligns with a previously held assumption that weakly-complexed Mn(III) species can be reactive oxidants [19].

In addition, we must stress that because Mn^{3+}/$MnOH^{2+}$ species were unstable, colloidal MnO_2 and Mn(II) should also be formed via a reaction of the type [22,23,57,63]:

$$2\ Mn^{(III)}OH^{2+} \rightarrow Mn^{(IV)}O_{2\ (s)} + Mn^{(II)} + 2H^+ \quad (3)$$

This was tested by tracking the time-resolved disproportionation of Mn(III) using UV-Vis spectrophotometry (Fig. 4a, b). From the characteristic absorbances of Mn(III)-PP complexes (λ_{max} = 258 nm) [9,14,23], MnO_2 colloids (λ_{max} = ~370 nm) [45,64–67], we find that disproportionation was considerably slower at high (1:5) than at low (1:2) Mn

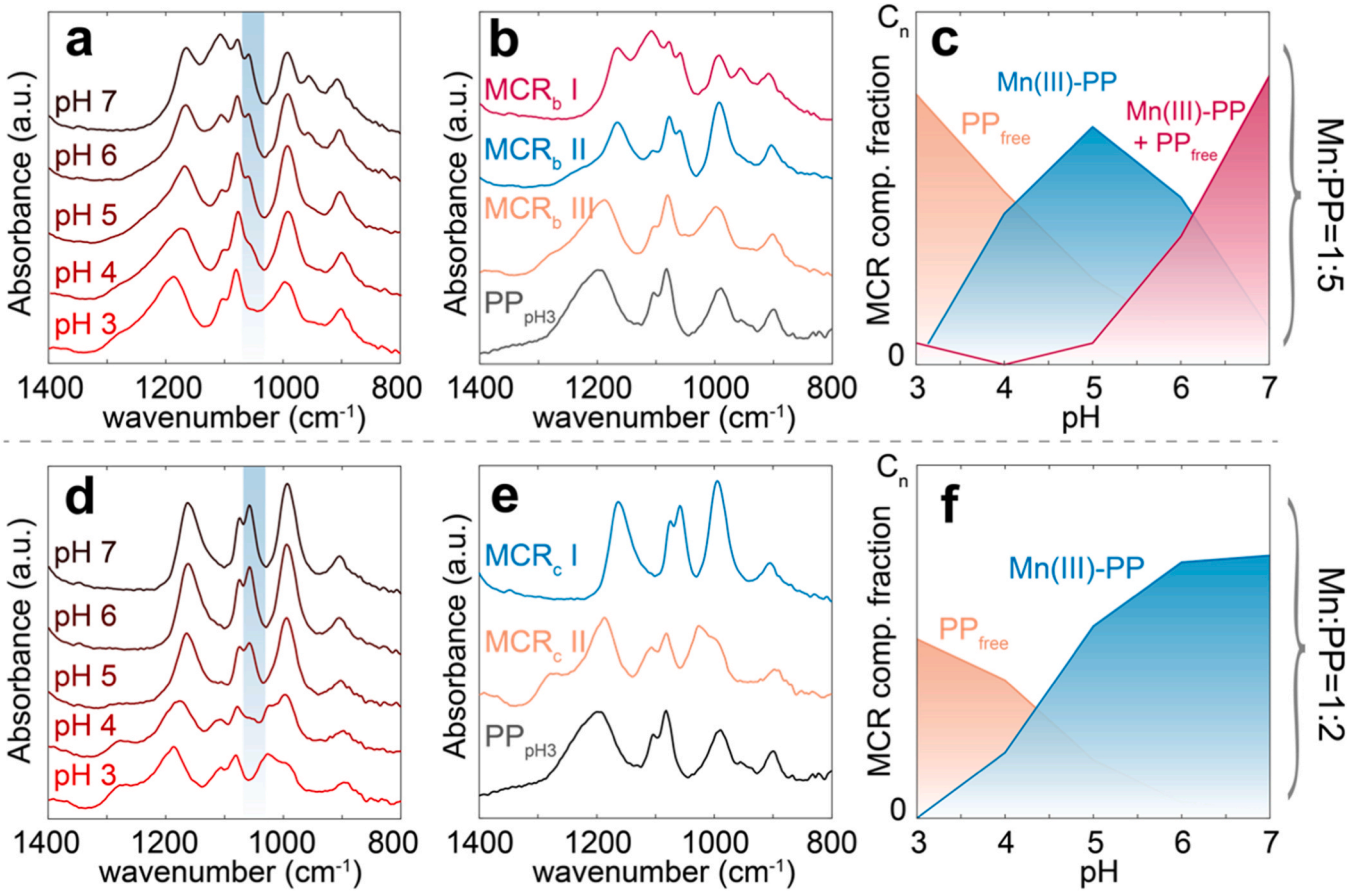

Fig. 3. Vibrational spectral response of 20 mM Mn(III) solutions at Mn:PP ratios of 1:5 (a) and 1:2 (a) from pH 3 to pH 7. MCR analyses for *n* components of (a) generated MCR_b spectral components in (b) and concentration profiles in (c). Those of (d) generated MCR_c spectral components of (e) and concentration profiles of (f).

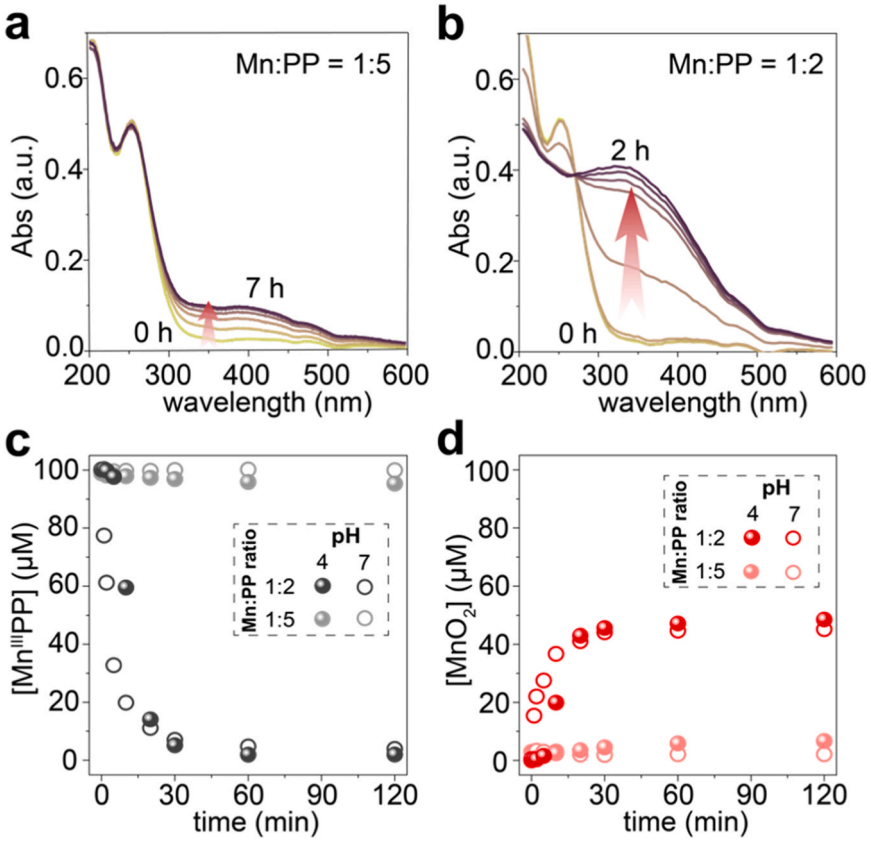

Fig. 4. Variations in UV-Vis spectra of Mn(III)-PP complexes at Mn(III):PP ratio of 1:5 (a) or 1:2 (b) at pH 4. Time-resolved concentrations showing the disappearance of Mn(III)-PP complexes (c) and the formation of MnO_2 colloids (d) at Mn:PP ratio of 1:2 or/and 1:5 and at pH 4 and 7.

(III)-PP ratios (Figs. S9-S10 and Fig. 4c, d). This can especially be appreciated from the contrasting changes in Mn(III)-PP concentration at these two ratios, and in the rise in the concentration of MnO_2 colloids. We also note that pH affected the reactivity of both $MnOH^{2+}$ and colloidal MnO_2, as lower pH favored CIP oxidation, a result that is in accordance with the increased redox potential of Mn(III)-PP solutions at lower pH (Fig. S2, Table S2). In addition to this, newly formed MnO_2 particles could efficiently contribute to CIP removal via surface complexation, and subsequently electron transfer [44,55,68,69]. This effect should be comparable to the results of an additional experiment (Fig. S8a) in which PP complexation had a slight inhibitory effect on CIP removal by synthetic δ-MnO_2.

Collectively, our findings revealed that Mn(III)-PP stability was central to CIP oxidation in mixed Mn(III)-PP-CIP solutions. Mn(III)-PP stability and its dissociation kinetics were largely controlled by Mn:PP ratios, while lower pH favored the participation of the redox-active $MnOH^{2+}$ species, as well as the subsequently produced MnO_2 colloids. In summary, the weakening of PP-Mn^{3+} bonds by changes in solution composition can trigger CIP oxidation.

4. Conclusions

By identifying the impact of PP complexation on the redox activity of Mn(III) species, our work identified stability regimes for CIP and potentially other related fluoroquinolone antibiotic contaminants in water. This knowledge was developed by recognizing that PP complexation limits the accessibility of reactive Mn to CIP functional groups, which is necessary for electron transfer.

Chelation with natural (in)organic ligands can promote Mn(III) mobility in nature, contrasting with colloidal oxides that tend to hinder transport. It should, however, be an essential aspect to consider along proton and ligand concentration gradients experienced by migrating bodies in aquatic and terrestrial environments. Notable settings include transitions across acid mine drainage, or acid rain run-off from highlands to rivers and lakes. As ideas on the occurrence of dissolved Mn(III) and its formation mechanisms are developing in environmental geochemistry [9] and pollution remediation [10], this work highlights that complexed Mn(III) species tend to destabilize when moving across oxic-anoxic interfaces in water columns. This phenomenon could even provide new insight into working with acidic wastewater by allowing dissolved Mn(III) species and MnO_2 colloids to remove contaminants in environmental engineering applications [70,71]. Changes in concentrations of Mn(III) stabilizing ligands and protons could help explain the challenges associated in detecting low concentrations of dissolved Mn (III) in natural waters [1,72]. From a broader aspect, local Mn cycling should not only impact carbon cycles via organic compounds oxidation/mineralization [73,74] but also the cycling of other elements, such as lead [75], uranium [19], and mercury [76].

These findings should also be readily extended to a wide range of naturally occurring ligands that can extend the lifetime of Mn(III). Examples include organic acids [7,22], biogenic siderophores [7,77], or dissolved organic matter [5]. This diversity of chelating organic ligands on stabilizing Mn(III) could be a challenge to shed light on Mn(III) reactivity in the oxidation process. Accounting for mechanisms of intermolecular electron transfer should also be considered, as differences in ligand affinities to Mn(III) may lead to diverse stability regimes for organic contaminants. As more remains to be known on the roles of Mn(III)-ligand complexes in natural environments, we should expect more detailed studies on their structure and reactivity. Developing this knowledge will also be increasingly vital for developing strategies for managing the environmental fate of antibiotics, a task that will ultimately contribute to better water quality and public health. Work along this line should, at the same time, contribute in advancing knowledge on the coupled biogeochemical cycles of manganese and carbon.

Environmental Implication

Aqueous Mn(III) species play important roles in degrading antibiotics released to the environment. This study demonstrates that ciprofloxacin, a predominant antibiotic contaminant, can be degraded when directly coordinated to Mn(III). However, degradation is inhibited if Mn (III) is complexed with strongly-binding ligands, such as pyrophosphate. Our research identified pH ranges where this competitive complexation stabilizes ciprofloxacin in water. These findings emphasize the importance of considering the inhibiting effects of pyrophosphate-like ligands on Mn(III)-driven oxidation of ciprofloxacin. This is especially vital for antibiotic transport monitoring programs aimed at improving water quality and public health.

CRediT authorship contribution statement

Jean-François Boily: Writing – review & editing, Writing – original draft, Supervision, Project administration, Funding acquisition, Conceptualization. **Tao Luo:** Data curation, Formal analysis, Methodology. **Tao Chen:** Writing – original draft, Methodology, Investigation, Formal analysis, Data curation, Conceptualization. **Yann Leroux:** Writing – original draft, Methodology, Formal analysis, Data curation. **Tra My Bui Thi:** Writing – review & editing, Writing – original draft, Methodology, Formal analysis, Data curation, Conceptualization. **Khalil Hanna:** Writing – review & editing, Writing – original draft, Supervision, Funding acquisition, Conceptualization.

Declaration of Competing Interest

The authors declare that they have no known competing financial interests or personal relationships that could have appeared to influence the work reported in this paper.

Acknowledgments

The authors wish to thank support from Swedish Research Council (2020-04853, 2024-04694) and FORMAS (2022-01246) to JFB, the French National Research Agency via the INFLOW project (ANR-21-CE29-0008-01) to KH and JFB, the CNRS (IRP CHEMICY 2022-2027) to KH and JFB, and a Région Bretagne for a mobility grant for an extended research stay at Umeå University to TMBT.

Appendix A. Supporting information

Supplementary data associated with this article can be found in the online version at doi:10.1016/j.jhazmat.2025.138373.

Data availability

Data will be made available on request.

References

[1] Trouwborst, R.E., Clement, B.G., Tebo, B.M., Glazer, B.T., Luther, G.W., 2006. Soluble Mn(III) in suboxic zones. Science 313, 1955–1957.
[2] Oldham, V.E., Mucci, A., Tebo, B.M., Luther, G.W., 2017. Soluble Mn(III)–L complexes are abundant in oxygenated waters and stabilized by humic ligands. Geochim Cosmochim Acta 199, 238–246.
[3] Lewis, B.L., Landing, W.M., 1991. The biogeochemistry of manganese and iron in the Black Sea. Deep Sea Res Part A Oceanogr Res Pap 38, S773–S803.
[4] Johnson, K.L., McCann, C.M., Wilkinson, J.L., Jones, M., Tebo, B.M., West, M., Elgy, C., Clarke, C.E., Gowdy, C., Hudson-Edwards, K.A., 2018. Dissolved Mn(III) in water treatment works: Prevalence and significance. Water Res 140, 181–190.
[5] Li, Q., Xie, L., Jiang, Y., Fortner, J.D., Yu, K., Liao, P., Liu, C., 2019. Formation and stability of NOM-Mn(III) colloids in aquatic environments. Water Res 149, 190–201.
[6] Li, H., Santos, F., Butler, K., Herndon, E., 2021. A critical review on the multiple roles of manganese in stabilizing and destabilizing soil organic matter. Environ Sci Technol 55, 12136–12152.
[7] Oldham, V.E., Owings, S.M., Jones, M.R., Tebo, B.M., Luther, G.W., 2015. Evidence for the presence of strong Mn(III)-binding ligands in the water column of the Chesapeake Bay. Mar Chem 171, 58–66.
[8] Jones, M.R., Luther, G.W., Tebo, B.M., 2020. Distribution and concentration of soluble manganese(II), soluble reactive Mn(III)-L, and particulate MnO_2 in the Northwest Atlantic Ocean. Mar Chem 226, 103858.
[9] Chen, T., Bui Thi, T.M., Luo, T., Cheng, W., Hanna, K., Boily, J.-F., 2024. Redox-driven formation of Mn(III) in ice. Environ Sci Technol 58, 15194–15201.
[10] Wang, X., Jones, M.R., Pan, Z., Lu, X., Deng, Y., Zhu, M., Wang, Z., 2024. Trivalent manganese in dissolved forms: occurrence, speciation, reactivity and environmental geochemical impact. Water Res 263, 122198.
[11] Kostka, J.E., Luther, G.W., Nealson, K.H., 1995. Chemical and biological reduction of Mn (III)-pyrophosphate complexes: potential importance of dissolved Mn (III) as an environmental oxidant. Geochim Cosmochim Acta 59, 885–894.
[12] Zhong, S., Zhang, H., 2020. Mn(III)-ligand complexes as a catalyst in ligand-assisted oxidation of substituted phenols by permanganate in aqueous solution. J Hazard Mater 384, 121401.
[13] Gao, Y., Jiang, J., Zhou, Y., Pang, S.Y., Jiang, C., Guo, Q., Duan, J.Bin, 2018. Does soluble Mn(III) oxidant formed in situ account for enhanced transformation of triclosan by Mn(VII) in the presence of ligands? Environ Sci Technol 52, 4785–4793.
[14] Webb, S.M., Dick, G.J., Bargar, J.R., Tebo, B.M., 2005. Evidence for the presence of Mn(III) intermediates in the bacterial oxidation of Mn(II). Proc Natl Acad Sci USA 102, 5558–5563.
[15] Hu, S., Zheng, L., Zhang, H., Chen, G., Yang, Y., Ouyang, Z., Chen, S., Gao, K., Liu, C., Wang, Q., Liu, T., 2023. Hematite-mediated Mn(II) abiotic oxidation under oxic conditions: pH effect and mineralization. J Colloid Interface Sci 636, 267–278.
[16] Chen, W.R., Liu, C., Boyd, S.A., Teppen, B.J., Li, H., 2013. Reduction of carbadox mediated by reaction of Mn(III) with oxalic acid. Environ Sci Technol 47, 1357–1364.
[17] Zhou, H., Zhong, S., Chen, J., Ren, S., Ren, W., Lai, B., Guan, X., Ma, T., Wang, S., Duan, X., 2024. Overlooked complexation and competition effects of phenolic contaminants in a Mn(II)/nitrilotriacetic acid/peroxymonosulfate system: inhibited generation of primary and secondary high-valent manganese species. Environ Sci Technol 58, 19080–19089.
[18] Sun, Y., Wang, C., May, A.L., Chen, G., Yin, Y., Xie, Y., Lato, A.M., Im, J., Löffler, F. E., 2023. Mn(III)-mediated bisphenol a degradation: mechanisms and products. Water Res 235, 119787.
[19] Wang, Z., Xiong, W., Tebo, B.M., Giammar, D.E., 2014. Oxidative UO_2 dissolution induced by soluble Mn(III). Environ Sci Technol 48, 289–298.
[20] Duckworth, O.W., Sposito, G., 2005. Siderophore-manganese (III) interactions. I. Air-oxidation of manganese(II) promoted by desferrioxamine B. Environ Sci Technol 39, 6037–6044.
[21] Y Wang, Y., Stone, A.T., 2008. Phosphonate- and carboxylate-based chelating agents that solubilize (hydr)oxide-bound Mn^{III}. Environ Sci Technol 42, 4397–4403.
[22] Kenneth Klewicki, J., Morgan, J.J., 1998. Kinetic behavior of Mn(III) complexes of pyrophosphate, EDTA, and citrate. Environ Sci Technol 32, 2916–2922.
[23] Qian, A., Zhang, W., Shi, C., Pan, C., Giammar, D.E., Yuan, S., Zhang, H., Wang, Z., 2019. Geochemical stability of dissolved Mn(III) in the presence of pyrophosphate as a model ligand: complexation and disproportionation. Environ Sci Technol 53, 5768–5777.
[24] Gunary, D., 1966. Pyrophosphate in soil; some physico-chemical aspects. Nature 210, 1297–1298.
[25] Sundareshwar, P.V., Morris, J.T., Pellechia, P.J., Cohen, H.J., Porter, D.E., Jones, B. C., 2001. Occurrence and ecological implications of pyrophosphate in estuaries. Limnol Oceano 46, 1570–1577.
[26] Torrent, J., Barberis, E., Gil-Sotres, F., 2007. Agriculture as a source of phosphorus for eutrophication in southern Europe. Soil Use Manag 23, 25–35.
[27] Yang, S., Shobnam, N., Sun, Y., Löffler, F.E., Im, J., 2024. The relative contributions of Mn(III) and Mn(IV) in manganese dioxide polymorphs to bisphenol A degradation. J Hazard Mater 461.
[28] Nico, P.S., Zasoski, R.J., 2001. Mn(III) center availability as a rate controlling factor in the oxidation of phenol and sulfide on δ-MnO_2. Environ Sci Technol 35, 3338–3343.
[29] Jia, D., Brigante, M., Zhang, C., Mailhot, G., 2023. Impact of Mn^{2+} in bisphenol A degradation by chelating agents-assisted manganese dioxide: mechanism understanding and efficiency evaluation. J Water Process Eng 56, 104388.
[30] Huo, X., Yi, H., Ma, D., Xu, F., Yan, H., Tang, L., Zeng, G., Lai, C., 2024. Reactive complexes mediated singlet oxygen production by MnO_2 catalyzed peracetic acid: characterization and DFT study. Chem Eng J 497, 154571.
[31] Lu, X., Wang, X., He, H., Liu, Q., Li, J., Zhao, Z., Yang, P., Pan, Z., Wang, Z., 2024. Bisphenol A degradation by manganese oxides at circumneutral pH: quantitative evaluation of dissolved Mn(III) species with pyrophosphate. J Hazard Mater, 137013.
[32] Hirsch, R., Ternes, T., Haberer, K., Kratz, K.L., 1999. Occurrence of antibiotics in the aquatic environment. Sci Total Environ 225, 109–118.
[33] K'oreje, K.O., Vergeynst, L., Ombaka, D., De Wispelaere, P., Okoth, M., Van Langenhove, H., Demeestere, K., 2016. Occurrence patterns of pharmaceutical residues in wastewater, surface water and groundwater of Nairobi and Kisumu city, Kenya. Chemosphere 149, 238–244.
[34] Aldred, K.J., Kerns, R.J., Osheroff, N., 2014. Mechanism of quinolone action and resistance. Biochemistry 53, 1565–1574.
[35] Redgrave, L.S., Sutton, S.B., Webber, M.A., Piddock, L.J.V., 2014. Fluoroquinolone resistance: mechanisms, impact on bacteria, and role in evolutionary success. Trends Microbiol 22, 438–445.

[36] Ma, D., Lai, C., Yi, H., Huo, X., Li, L., Zhang, M., Xu, F., Yan, H., Hu, S., Luo, Y., 2025. Confinement strategies for the design of efficient heterogeneous Fenton-like catalysts: from nano-space to atomic scale. Coord Chem Rev 522.
[37] Yan, H., Lai, C., Liu, S., Wang, D., Zhou, X., Zhang, M., Li, L., Ma, D., Xu, F., Huo, X., Tang, L., Yan, M., Nie, J., Fan, X., 2023. Insight into the selective oxidation behavior of organic pollutants via Ni-N_4-C mediated electron transfer pathway. Chem Eng J 473, 145253.
[38] Martin, S., Shchukarev, A., Hanna, K., Boily, J.F., 2015. Kinetics and mechanisms of ciprofloxacin oxidation on hematite surfaces. Environ Sci Technol 49, 12197–12205.
[39] Zhang, H., Huang, C.H., 2005. Oxidative transformation of fluoroquinolone antibacterial agents and structurally related amines by manganese oxide. Environ Sci Technol 39, 4474–4483.
[40] Sun, B., Li, D., Linghu, W., Guan, X., 2018. Degradation of ciprofloxacin by manganese(III) intermediate: insight into the potential application of permanganate/bisulfite process. Chem Eng J 339, 144–152.
[41] Gao, Y., Zhou, Y., Pang, S.Y., Jiang, J., Shen, Y.M., Song, Y., Duan, J.Bin, Guo, Q., 2021. Enhanced peroxymonosulfate activation via complexed Mn(II): a novel non-radical oxidation mechanism involving manganese intermediates. Water Res 193, 116856.
[42] Xu, K., Dong, H., Li, M., Qiang, Z., 2018. Quinone group enhances the degradation of levofloxacin by aqueous permanganate: kinetics and mechanism. Water Res 143, 109–116.
[43] Morgan, J.J., Schlautman, M.A., Bilinski, H., 2021. Rates of abiotic Mn^{II} oxidation by O_2: influence of various multidentate ligands at high pH. Environ Sci Technol 55, 14426–14435.
[44] Li, Q., Schild, D., Pasturel, M., Lützenkirchen, J., Hanna, K., 2022. Alteration of birnessite reactivity in dynamic anoxic/oxic environments. J Hazard Mater 433, 128739.
[45] Soldatova, A.V., Romano, C.A., Tao, L., Stich, T.A., Casey, W.H., Britt, R.D., Tebo, B.M., Spiro, T.G., 2017. Mn(II) oxidation by the multicopper oxidase complex Mnx: a coordinated two-stage Mn(II)/(III) and Mn(III)/(IV) mechanism. J Am Chem Soc 139, 11381–11391.
[46] Soldatova, A.V., Tao, L., Romano, C.A., Stich, T.A., Casey, W.H., Britt, R.D., Tebo, B.M., Spiro, T.G., 2017. Mn(II) oxidation by the multicopper oxidase complex Mnx: a binuclear activation mechanism. J Am Chem Soc 139, 11369–11380.
[47] Guan, X.H., Liu, Q., Chen, G.H., Shang, C., 2005. Surface complexation of condensed phosphate to aluminum hydroxide: an ATR-FTIR spectroscopic investigation. J Colloid Interface Sci 289, 319–327.
[48] Jaumot, J., de Juan, A., Tauler, R., 2015. MCR-ALS GUI 2.0: new features and applications. Chemom Intell Lab Syst 140, 1–12.
[49] Malinowski, E.R., 1977. Determination of the number of factors and the experimental error in a data matrix. Anal Chem 49, 612–617.
[50] Islam, M.A., Rahman, M.M., 2013. Soluble colloidal manganese dioxide: formation, identification and prospects of application. Colloid J 75, 538–542.
[51] Lu, P., Zhang, G., Apps, J., Zhu, C., 2022. Comparison of thermodynamic data files for PHREEQC. Earth Sci Rev 225, 103888.
[52] Sun, B., Rao, D., Sun, Y., Guan, X., 2016. Auto-accelerating and auto-inhibiting phenomena in the oxidation process of organic contaminants by permanganate and manganese dioxide under acidic conditions: effects of manganese intermediates/products. RSC Adv 6, 62858–62865.
[53] Quintas, M., Brandão, T.R.S., Silva, C.L.M., 2007. Modelling autocatalytic behaviour of a food model system—sucrose thermal degradation at high concentrations. J Food Eng 78, 537–545.
[54] Peng, Y., Zhang, Q., Ren, W., Duan, X., Ding, L., Jing, Y., Shao, P., Xiao, X., Luo, X., 2023. Thermodynamic and kinetic behaviors of persulfate-based electron-transfer regime in carbocatalysis. Environ Sci Technol 57, 19012–19022.
[55] Zhang, H., Chen, W.R., Huang, C.H., 2008. Kinetic modeling of oxidation of antibacterial agents by manganese oxide. Environ Sci Technol 42, 5548–5554.
[56] Huang, J., Zhong, S., Dai, Y., Liu, C.C., Zhang, H., 2018. Effect of MnO_2 phase structure on the oxidative reactivity toward bisphenol A degradation. Environ Sci Technol 52, 11309–11318.
[57] Gordienko, V.I., Sidorenko, V.I., Mikhailyuk, Y.I., 1970. Amperometric investigation of Mn (III) pyrophosphate complexes. Russ J Inorg Chem 15, 1241–1244.
[58] Asl, H.Y., Manthiram, A., 2020. Reining in dissolved transition-metal ions. Science 369 (1979), 140–141.
[59] Ta, H.T.T., Tieu, A.K., Zhu, H., Yu, H., Ta, T.D., Wan, S., Tran, N.V., Le, H.M., 2018. Chemical origin of sodium phosphate interactions on iron and iron oxide surfaces by first principle calculations. J Phys Chem C 122, 635–647.
[60] Vazquez, G.J., Dodge, C.J., Francis, A.J., 2007. Interactions of uranium with polyphosphate. Chemosphere 70, 263–269.
[61] Nedyalkova, M., Antonov, V., 2018. Manganese oxalates - structure-based Insights. Open Chem 16, 1176–1183.
[62] Stone, A.T., 1987. Reductive dissolution of manganese(III/IV) oxides by substituted phenols. Environ Sci Technol 21, 979–988.
[63] Baral, S., Lume-Pereira, C., Janata, E., Henglein, A., 1986. Chemistry of colloidal manganese oxides. 3. Formation in the reaction of hydroxyl radicals with Mn^{2+} ions. J Phys Chem 90, 6025–6028.
[64] Kim, H., Watthanaphanit, A., Saito, N., 2016. Synthesis of colloidal MnO_2 with a sheet-like structure by one-pot plasma discharge in permanganate aqueous solution. RSC Adv 6, 2826–2834.
[65] Soldatova, A.V., Butterfield, C., Oyerinde, O.F., Tebo, B.M., Spiro, T.G., 2012. Multicopper oxidase involvement in both Mn(II) and Mn(III) oxidation during bacterial formation of MnO_2. J Biol Inorg Chem 17, 1151–1158.
[66] Wei, W., Wang, A., Guo, K., He, S., Li, A., Kang, X., Fang, J., 2022. Enhanced degradation of micropollutants by UV/freshly formed colloidal MnO_2: reactive species, kinetics and pathways. Appl Catal B 313, 121441.
[67] Soldatova, A.V., Balakrishnan, G., Oyerinde, O.F., Romano, C.A., Tebo, B.M., Spiro, T.G., 2019. Biogenic and synthetic MnO_2 nanoparticles: size and growth probed with absorption and Raman spectroscopies and dynamic light scattering. Environ Sci Technol 53, 4185–4197.
[68] Sun, B., Xiao, Z., Dong, H., Ma, S., Wei, G., Cao, T., Guan, X., 2019. Bisulfite triggers fast oxidation of organic pollutants by colloidal MnO_2. J Hazard Mater 363, 412–420.
[69] Li, Q., Pokharel, R., Zhou, L., Pasturel, M., Hanna, K., 2020. Coupled effects of Mn (II), pH and anionic ligands on the reactivity of nanostructured birnessite. Environ Sci Nano 7, 4022–4031.
[70] Tian, S., Ma, Y., Xu, Y., Jiang, S., Ma, J., Lin, Y., Wen, G., 2024. Efficient degradation of organic contaminants by activated permanganate with metal sulfides: in situ generation of Mn(III). ACS ES T Eng 4, 683–693.
[71] Liu, H., Dai, X., Kong, L., Sui, C., Nie, Z., Liu, Y., Cai, B., Ni, S.Q., Boczkaj, G., Zhan, J., 2023. Ball milling treatment of Mn_3O_4 regulates electron transfer pathway for peroxymonosulfate activation. Chem Eng J 467, 143339.
[72] Madison, A.S., Tebo, B.M., Mucci, A., Sundby, B., Luther, G.W., 2013. Abundant porewater Mn(III) is a major component of the sedimentary redox system. Science (1979) 341, 875–878.
[73] Chang Chien, S.W., Chen, H.L., Wang, M.C., Seshaiah, K., 2009. Oxidative degradation and associated mineralization of catechol, hydroquinone and resorcinol catalyzed by birnessite. Chemosphere 74, 1125–1133.
[74] Butterfield, C.N., Soldatova, A.V., Lee, S.W., Spiro, T.G., Tebo, B.M., 2013. Mn(II, III) oxidation and MnO_2 mineralization by an expressed bacterial multicopper oxidase. Proc Natl Acad Sci USA 110, 11731–11735.
[75] Wang, Xingxing, Wang, Q., Yang, P., Wang, Xiaoming, Zhang, L., Feng, X., Zhu, M., Wang, Z., 2020. Oxidation of Mn(III) species by Pb(IV) oxide as a surrogate oxidant in aquatic systems. Environ Sci Technol 54, 14124–14133.
[76] Zhang, S., Li, B., Chen, Y., Zhu, M., Pedersen, J.A., Gu, B., Wang, Z., Li, H., Liu, J., Zhou, X.Q., Hao, Y.Y., Jiang, H., Liu, F., Liu, Y.R., Yin, H., 2023. Methylmercury degradation by trivalent manganese. Environ Sci Technol 57, 5988–5998.
[77] Szabó, O., Farkas, E., 2011. Characterization of Mn(II) and Mn(III) binding capability of natural siderophores desferrioxamine B and desferricoprogen as well as model hydroxamic acids. Inorg Chim Acta 376, 500–508.